International Journal of Nanomedicine

Dovepress
open access to scientific and medical research

Open Access Full Text Article

ORIGINAL RESEARCH

Development of Drug Dual-Carriers Delivery System with Mitochondria-Targeted and pH/Heat Responsive Capacity for Synergistic Photothermal-Chemotherapy of Ovarian Cancer

This article was published in the following Dove Press journal:
International Journal of Nanomedicine

Xiaoxia Guo[1,*]
Jie Mei[1,*]
Chunping Zhang[2]

[1]Department of Obstetrics and Gynecology, Sichuan Academy of Medical Sciences and Sichuan Provincial People's Hospital, Chengdu 610041, Sichuan, People's Republic of China; [2]The Center of Clinical Laboratory, Sichuan Great Master Diagnostics Co. Ltd, Chengdu 611731, Sichuan, People's Republic of China

*These authors contributed equally to this work

Purpose: Multifunctional drug delivery systems (DDS) are emerging as a new strategy to highly treat malignant tumors. The aim of this study is to develop a drug dual-carriers delivery system (DDDS) using the natural protein ferritin (FRT) and a nanoscale graphene oxide (NGO) as dual-carriers.

Methods: The FRT is a pH-sensitive hollow cage protein with disassembly and reassembly properties and the NGO has a large surface area and a photothermal effect by which it can load and release drugs under near-infrared irradiation (NIR). Due to these unique features, the NGO loaded the anticancer drug resveratrol (RSV) and the conjugated mitochondrion targeted molecule IR780 as IR780-NGO-RSV (INR), the first drug delivery platform. Next, the INR was capsulated by FRT to form the DDDS INR@FRT which was applied for synergistic photothermal-chemotherapy of ovarian cancer.

Results: Through a series of characterizations, INR@FRT showed a uniform nanosphere structure and remarkable stability in physiological condition. Heat/pH 5.0 was confirmed to trigger RSV release from the INR@FRT. After taken up by cells, INR@FRT located to the lysosomes where the acidic environment triggered INR release. INR targeted the mitochondrion and released RSV to directly react with organelles, which in turn decreased the mitochondrion membrane potential and caused cell apoptosis. In-vivo experiments showed that INR@FRT combined with NIR irradiation displayed remarkable tumor suppression with a high survival rate after 60 days of treatment. Finally, the biocompatibility of INR@FRT was demonstrated in vitro and in vivo.

Conclusion: These results highlight the immense potential of INR@FRT as a type of DDDS for the treatment of tumors.

Keywords: resveratrol, apoptosis, drug dual-carriers delivery system, mitochondrion targeting, pH/heat-triggered tumor therapy

Introduction

Ovarian cancer poses a huge threat to women's health. Although significant progress has been made to cure it, huge challenges still remain. Common methods for the treatment of ovarian cancer mainly include surgery and systemic chemotherapy.[1–3] However, the treatment effect is still not ideal and recurrence is high. Additionally, currently used chemotherapy drugs have some disadvantages such as poor water solubility, rapid elimination of small molecules, lack of specific

Correspondence: Chunping Zhang
The Center of Clinical Laboratory, Sichuan Great Master Diagnostics Co. Ltd, No. 8, Anhe the Second Road, Hi-Tech Industrial Development Zone, Chengdu 611731, Sichuan, People's Republic of China
Tel +86-189 8008 6040
Email zcpcn7894@163.com

submit your manuscript | www.dovepress.com
DovePress
http://doi.org/10.2147/IJN.S226517

targeting, and systemic toxicity caused by large doses.[4–7] Therefore, new chemical and pharmaceutical preparations, such as multifunctional drug delivery systems (DDS), are expected to significantly improve the effects of chemotherapy.[8–14]

In the past few decades, there have been a large number of reports on the use of nanoparticle-based DDS for cancer treatment.[15–17] Compared to free small molecule chemotherapy drugs, DDS shows high bioavailability, low systemic side effects, and rich surface functional modification sites.[9,17] To date, DDS based on a variety of materials such as silica nanoparticles, carbon-based materials, liposomes, proteins, nanogels, etc., have been developed.[18–23] Most of them can be controllably stimulated to release drug, which prevents the off-target release and improves the therapy efficiency.[24–26] However, several shortcomings in DDS limit their applications: 1) Drug leakage may be easily stimulated during delivery of the drug from the bloodstream to tumor organelles; 2) Drugs released in the cytoplasm have no target organelles, which may influence the therapy effect. Therefore, to overcome these problems, new strategies are proposed.

In this study, we developed a drug dual-carriers delivery system (DDDS) based on common-used drug carriers, ferritin (FRT) and nanoscale graphene oxide (NGO). Ferritin is a natural protein and has 24 subunits which assemble into a hollow cage-like nanostructure and disassembles in acid and neutral conditions.[27–30] NGO is an excellent drug carrier as it has a large surface area, good drug loading ratio, and near-infrared (NIR) photothermal-triggered drug release.[31–37] In this DDDS, NGO, the first carrier of the highly loaded resveratrol (RSV), linked with mitochondrion targeted molecule IR780 to form INR. Next, ferritin, the second carrier capsulated the INR via the disassembly of FRT under acidic conditions. The drug delivery process consisted of the following steps: 1) DDDS uptake by cells and was carried by lysosomes (acidic conditions); this denatured FRT to release INR into the cytoplasm; 2) INR targeted the mitochondrion and NIR-released RSV to directly react with the target organelle. In this design, the drug is released only in the presence of two stimuli (acid and heat) and avoids drug leakage during delivery in the circulatory system. Additionally, the first carrier can be endowed with target organelle features, which can enhance the therapeutic effect. In-vitro and in-vivo experiments demonstrated that the prepared DDDS had excellent ovarian cancer therapy effect with excellent biocompatibility.

Materials and Methods

Materials

Graphene oxide powder was purchased from Nanjing XF NANO Materials Tech Co., Ltd (China). Mitotracker red, Lysotracker red, Calcein AM/PI kit, Annexin V-FITC/PI apoptosis staining kit were purchased from Solarbio (Beijing, China). IR-780 iodide (IR780), ferritin (FRT) from equine spleen, resveratrol (RSV, ≥99%), N-(3-dimethylaminopropyl)-N′-ethylcarbodiimidehydrochloride (EDC), N-hydroxysuccinimide (NHS) and 6-diamidino-2-phenylindole (DAPI) were purchased from Sigma-Aldrich (USA). All other chemicals used in the study were from Aladdin (Shanghai, China).

Cell Culture and Animal Models

The human ovarian cancer cell line SKOV-3 was purchased from American Type Culture Collection (ATCC, Manassas, VA, USA). The cells were cultured in DMEM complete media containing 10% fetal bovine serum, 1% penicillin-streptomycin, and in a 37°C constant temperature humidified carbon dioxide incubator. 5–8 weeks female Balb/c nude mice were purchased from Charles River Laboratories (Beijing, China). A SKOV-3 tumor xenograft model was constructed by subcutaneous injection of cell suspension (10^7 cells). All animal experiments were strictly in accordance with the Laboratory Animal Care and Protection Guidelines of Sichuan Academy of Medical Sciences and approved by the Ethics Committee of the Sichuan Academy of Medical Sciences.

Preparation and Characterization of INR@FRT

Firstly, GO powder (10 mg) was added to distilled water (5 mL) and sonicated for 12 h under an ice bath. Thereafter, the mixture was centrifuged at 12,000 rpm to collect nanoscale GO (NGO) in the supernatant. IR780 was mixed with NGO (w/w=1:1), and then EDC (8 mM) and NHS (10 mM) were sequentially added, and stirred at room temperature for 3 hrs. Then, the resulting mixture was dialyzed against distilled water for 24 hrs to remove excess chemicals to obtain an IR780-linked NGO (IR780-NGO, IN). For drug loading, 4 mg/mL of RSV solution (dissolved in DMSO) was added to the IR780-NGO solution (2 mg/mL) at 4°C and stirred for 6 h. The mixture was then dialyzed against distilled water (MW cutoff = 10 kDa) to remove unbound RSV and DMSO solvent to give purified RSV-loaded IR780-NGO (IR780-NGO-RSV, INR). The

concentration of bound RSV was measured by UV-vis spectroscopy (Perkin-Elmer, USA) at 306 nm.

Next, 1 mg/mL of FRT was dissolved in a buffer solution at pH 5.0 and gently stirred at room temperature for 30 min to ensure complete disassembly of the FRT. The INR was then added to the FRT solution, stirred for 10 min, and then the pH of the solution was adjusted to neutral with stirring. The resulting solution was then dialyzed against saline overnight to remove free drug and chemicals to give an INR-loaded FRT (INR@FRT). The morphology and size of the prepared nanoparticles were determined by atomic force microscopy (AFM, Agilent Technologies, Inc.) and Zetasizer (NanoZS; Malvern Instruments, Malvern, UK), respectively.

pH/Heat Triggered Drug Release Study

Place the INR@FRT solution in a dialysis tube (MW cut-off = 10 kDa) in a different pH release medium (25 mL PBS) with or without NIR irradiation (808 nm, 0.3 W/cm^2, 3 min) and stir (100RPM). At different time points, 1 mL of solution was removed from the released media and replaced with the same volume of fresh media. The amount of RSV in the removed solution was measured using a UV-vis spectrophotometer. The drug loading rate (DLR, %) was estimated by the following formula: DLR = (Wd/Wc) x 100%, where Wd is the weight of the drug determined by a UV-vis spectrophotometer and Wc is the weight of the carrier.

Cell Uptake and Intracellular Location

The fluorescent dye fluorescein isothiocyanate (FITC) was used to label NR@FRT and INR@FRT. In brief, 1 mg FITC was dissolved in 0.5 mL DMSO and then mixed with the nanoparticles with slight stir for 30 min. Afterwards, the mixture was dialyzed at deionized water for 24 h to remove the free FITC, resulting in FITC-labeled nanoparticles. The cells were seeded at a density of 1 × 10^5 cells/mL onto a confocal culture dish and incubated at 37°C for 12 hrs. FITC-labeled NR@FRT and INR@FRT were added to the cell culture medium. After 4 h of incubation, the cells were washed three times with PBS,[38] fixed with 4% paraformaldehyde for 15 min, and then stained with DAPI, Lysotracker Red, Mitotracker Red, respectively. Fluorescence signals in the cells were observed using a confocal laser scanning microscope (Nikon A1R MP, Japan). In addition, flow cytometry (FCM) was further used to assess the fluorescent signal of dyes (including FITC, Mitotracker Red, Lysotracker Red) in cells. The treated cells were also observed by bio-TEM.

In vitro Cancer Photothermal – Chemotherapy

SKOV-3 cells were seeded in 96-well plates (2 x 10^4 cells/well) and incubated for 24 hrs. Different concentrations of RSV, IN@FRT, NR@FRT, INR@FRT were added directly to fresh cell culture medium and incubated for 4 h in an incubator. Then, the plate was taken out, the old medium was gently removed, and fresh medium was added, and the cells were irradiated with an 808 nm laser (0.3 W/cm^2, 3 min). Put it in the incubator again and continue to culture for 24 h or 48 h. At the end, cell viability was measured using the CCK-8 assay. In addition, thermal images of the treated cells and corresponding temperature changes were recorded.

In addition, the photothermal therapy effect of INR@FRT on SKOV-3 cells was further verified by calcein AM and propidium iodide (PI) co-staining. As with the above cell treatment method, SKOV-3 cells were subjected to NIR irradiation and continued to culture for 48 h after RSV, IN@FRT, NR@FRT, INR@FRT treatment. Then, it was stained with a mixed solution of calcein AM and PI at room temperature for 15 mins, and then washed three times with PBS. The stained cells were examined under a laser scanning confocal microscope. The excitation wavelength of calcein AM was set to 490 nm, and the excitation wavelength of PI was set to 535 nm.

Apoptosis and Mitochondrial Membrane Potential (MMP) Detection

Cells were seeded in 6-well plates (1 x 10^4 cells/well) for 24 h, and then treated with RSV, IN@FRT, INR @FRT, NR@FRT + NIR, INR@FRT + NIR (with the same RSV concentration 40 μg/mL) for 48 h. The cells were then collected, washed, and double stained with the Annexin V-FITC/PI kit, and then statistically analyzed for FITC and PI fluorescence in the cells using FCM. The cells treated in the same manner as above were also stained with a potential sensitive dye (rhodamine 123), and then the changes in cellular MMP were evaluated by FCM analysis.

In vivo Blood Circulation and Biodistribution Study

The normal mice were intravenous injected with RSV and INR@FRT. And then, blood samples were collected at

different times from the orbital plexus. Each blood sample was dissolved in 900 μL of lysis buffer. The concentration of RSV and INR@FRT in the blood was determined by RSV absorbance spectra of each solubilized blood sample by an UV−Vis spectrometer. The sample concentrations are defined as the percentage of injected dose per gram of tissue (ID%/g). Biodistribution in tumor and major organs was performed in tumor-bearing mice. The tumor tissues and major organs (including heart, liver, spleen, lungs and kidney) were weighed and digested by aqua regia solution overnight at 24 hrs post-intravenous injection of NR@FRT and INR@FRT, respectively. The concentration of NR@FRT and INR@FRT in the collected tissue was determined by RSV absorbance spectra of each solubilized tissue by an UV−Vis spectrometer. The sample concentrations are defined as the percentage of injected dose per gram of tissue (ID%/g).

In vivo Cancer Photothermal-Chemotherapy

Nude mice bearing SKOV-3 subcutaneous xenografts were randomized into 7 groups (n = 5), and then injected with PBS, RSV, IN@FRT, NR@FRT, INR@FRT, NR@FRT + NIR and INR@FRT + NIR (containing the same RSV concentration with 5 mg/kg) via the tail vein. The samples were injected two times at day 1 and day 3. At 12 and 24 hrs after the intravenous administration of the samples, the tumor area was irradiated with a 3 min NIR laser (808 nm, 0.3 W/cm^2), respectively. Mice were imaged using a NIR thermography system (FLUKE) during laser irradiation. The tumor size and weight of the mice were tested every 3 days during treatment. Tumor volume = (tumor length) x (tumor width)^2/2. The relative tumor volume is equal to the tumor volume at a given time point divided by the tumor volume prior to the initial treatment. At the end, the tumor and major organs of

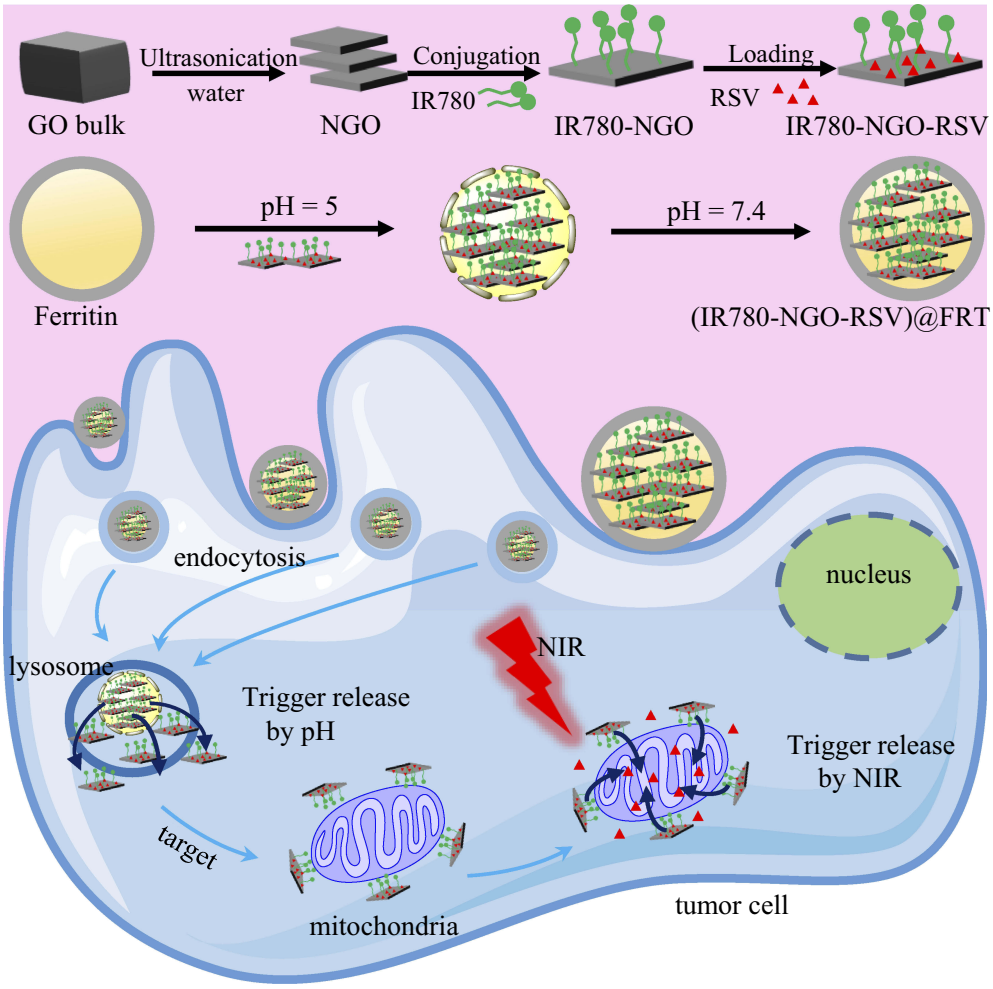

Figure 1 Schematic representation of the synthesis of drug dual-delivery system INR@FRT for synergistic photothermal-chemotherapy of ovarian cancer.
Abbreviations: GO, graphene oxide; NGO, nanosized graphene oxide; IR780, IR-780 iodide; NIR, near-infrared; RSV, resveratrol; FRT, ferritin.

the heart, liver, spleen, lungs and kidneys of these mice were collected, fixed in 4% formalin, embedded in paraffin, stained with H&E, and examined under a digital microscope.

Statistical Analysis

All statistics are expressed as mean ± SD. Statistical significance was tested by two-tailed Student's *t* test. $P<0.05$ or $P<0.01$ was considered statistically significant.

Results and Discussion

Synthesis and Characterization of INR@FRT

To synthesize a DDDS, INR@FRT, firstly, biocompatible NGO as the first carrier was prepared through ultrasonication. Then, the NGO was conjugated with IR780, a mitochondrion specific-targeted molecule, and loaded RSV, an anticancer drug, to form a nanocomposite (INR). FRT was the second carrier to capsulate the INR via the pH-responsive disassembly and reassembly of FRT. The DDDS was used for synergistic photothermal-chemotherapy of ovarian cancer in-vitro and in-vivo (Figure 1). The morphology of the nanoparticles was characterized by AFM, which showed that the NGO and the INR were sheet-like and the INR@FRT was a sphere-like structure (Figure 2A–F); their heights were ~1 nm, ~3 nm, and ~16 nm, respectively (Figure 2B, D, F). Additionally, the DLS analysis showed that the sizes of NGO, INR, and INR@FRT were ~10 nm, ~13 nm, and ~26 nm, respectively (Figure 2G). These results indicate that after conjugation of IR780 and RSV loading followed by FRT capsulation, the

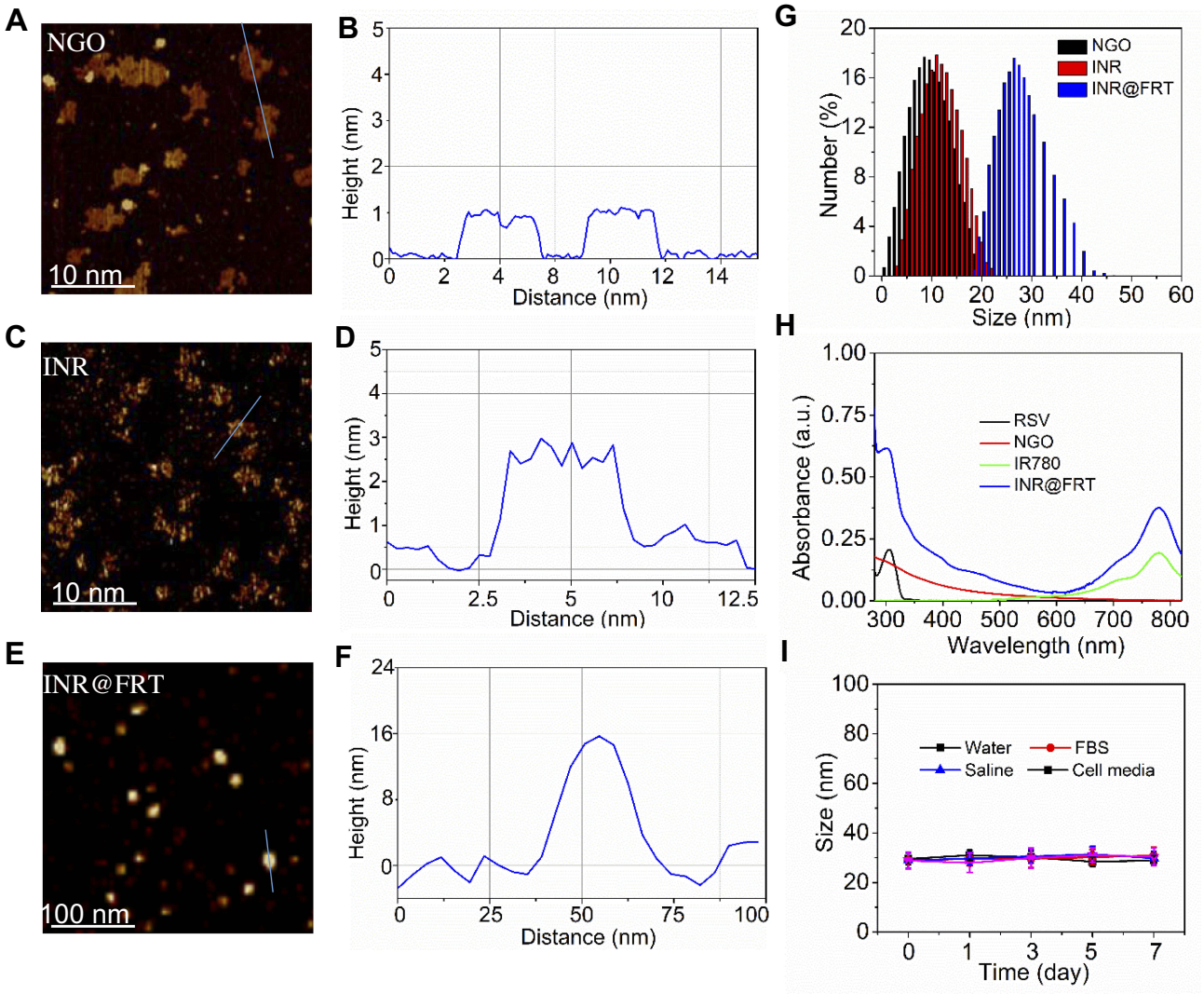

Figure 2 (**A** and **B**) The AFM image and height profile of NGO. (**C** and **D**) The AFM image and height profile of INR. (**E** and **F**) The AFM image and height profile of INR@FRT. (**G**) The size distribution of NGO, INR and INR@FRT. (**H**) The absorption spectra of RSV, NGO, IR780, and INR@FRT, respectively. (**I**) The hydrodynamic particle size change of INR@FRT in various media including water, FBS, cell media, and saline over 7 days.

Abbreviations: NGO, nanosized graphene oxide; IR780, IR-780 iodide; RSV, resveratrol; FRT, ferritin; AFM, atom force microscopy; FBS, fetal bovine serum.

size increased sequentially. Moreover, the UV-VIS spectrum of INR@FRT showed the absorbance peak of RSV at 306 nm and IR780 at 780 nm (Figure 2H); this demonstrated the successful loading of RSV and IR780 on to the DDDS. After 7 days, it was found the INR@FRT showed no obvious size change in water, FBS, saline, and cell media (Figure 2I), suggesting that the INR@FRT was stable in the physiological environment. The RSV loading ratio was ~132% (W/W).

The Photothermal Effect of INR@FRT

As shown in Figure 3A, the temperature profile of INR@FRT had a quick-rising phase and reached a plateau of 61.5°C within 3 min of irradiation (808 nm, 0.3 W/cm^2). As a control, the maximum temperature of FRT and NR@FRT reached 26.5°C and 42.3°C, respectively, under the same conditions. These results indicated that the INR@FRT has an excellent photothermal effect likely due to the conjugation of IR780 and NGO and that IR780 provided the most contribution. Additionally, the NR@FRT and INR@FRT retained their initial photothermal effect even after 5 cycles of NIR irradiations (Figure 3B), suggesting that both of them have great photostability. Furthermore, when the INR@FRT was incubated in different temperatures, from 25°C to 85°C, it showed a stable size at <65°C and increasing size at >80°C (Figure 3C), likely due to the great resistance of FRT to denaturants including high temperatures.[30,39]

pH/Heat Triggered Drug Release Study

As reported in previous studies,[20,30] FRT and NGO, as drug carriers, were pH and heat sensitive, respectively, and these two factors were applied for this study on drug triggered release of INR@FRT. As shown in Figure 4A, over 24 hrs, from a pH of 5.0 to 9.0, INR@FRT seldom showed RSV release. When combining with NIR irradiation, INR@FRT at a pH of 5.0 showed about 60% accumulated RSV release after 24 h, and interestingly, in pH 7.4, it still displayed no significant RSV release (Figure 4B). These results indicated that

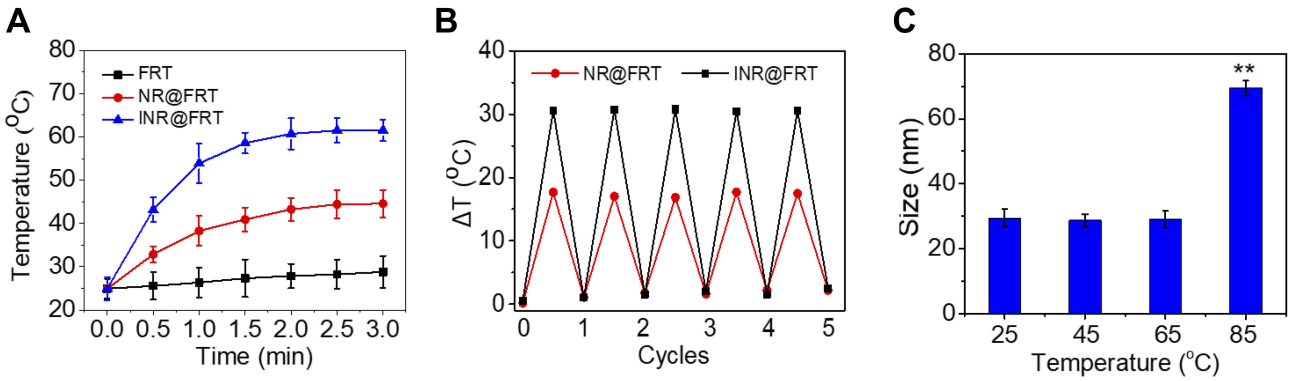

Figure 3 (**A**) Photothermal heating curves of FRT, NR@FRT and INR@FRT solution under 3 min 808 nm laser irradiation (0.3 W/cm^2). (**B**) Temperature variations of NR@FRT and INR@FRT after the continuous irradiations of 3 min 808 nm laser for 5 cycles. (**C**) The size change of INR@FRT from 25°C to 85°C. **P<0.01, vs other groups.
Abbreviations: NGO, nanosized graphene oxide; IR780, IR-780 iodide; RSV, resveratrol; FRT, ferritin.

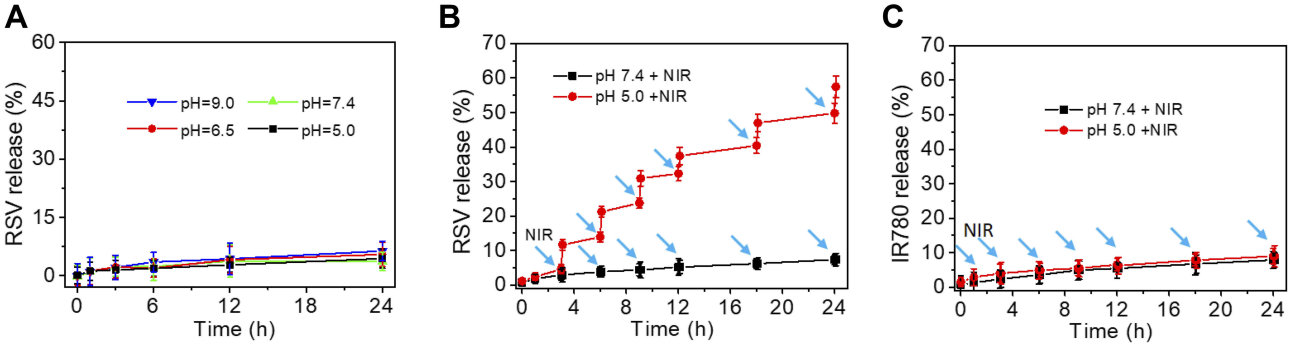

Figure 4 (**A**) Release kinetics of RSV from INR@FRT in pH 9.0, 7.4, 6.5 and 5.0. (**B**) Release kinetics of RSV from INR@FRT in PBS buffer (pH = 7.4 and 5.0) with 3 min NIR irradiation (808 nm, 0.3 W/cm^2). (**C**) Release kinetics of IR780 from INR@FRT in pH 7.4 and 5.0 combined with 3 min NIR irradiation (808 nm, 0.3 W/cm^2). The arrows represent the NIR irradation.
Abbreviations: IR780, IR-780 iodide; RSV, resveratrol.

acidity and NIR irradiation-induced heat can highly trigger RSV release from INR@FRT. The pH values in cell lysosomes and the normal physiological environment are 5.0 and 7.4, respectively.[20] Additionally, FRT is reported to disassemble into a hollow porous nanosphere under acidic conditions and reassemble into a sealed hollow nanosphere under neutral conditions.[28] Thus, the stepwise release process is 1) FRT denatured to release the INR in acidic conditions 2) NGO released RSV under NIR irradiation. Either pH 5.0 or NIR irradiation alone could not trigger RSV release from the DDDS. This strategy can help avoid drug leakage caused by a single factor. Additionally, IR780 cannot be released from INR@FRT at a pH of 7.4 and 5.0 combined with NIR irradiation, as shown in Figure 4C, indicating the stability of the IR780 conjugation in the DDDS.

Cell Uptake and Intracellular Distribution of INR@FRT

The cell uptake and intracellular distribution of INR@FRT were analyzed by confocal microscopy and flow cytometry. As shown in Figure 5A–C, the FITC-labeled NR@FRT and INR@FRT incubated with cells for 4 h showed no significant difference of fluorescence intensity in the cytoplasm (Figure 5A and B), as well as cell uptake according to the flow cytometry (Figure 5C), indicating that both could enter cells via endocytosis without specificity. After entering cells, NR@FRT and INR@FRT were both carried into lysosomes, as shown in Figure 5A. However, the INR@FRT displayed a greater intensity of yellow fluorescence (FITC green and Mitotracker red fused color) when compared to NR@FRT (Figure 5B). The statistical results in Figure 5D additionally confirmed the organelle distribution of INR@FRT. Moreover, the distribution of INR@FRT within the organelles was further confirmed using Bio-TEM, which showed retained nanoparticles in the mitochondria and lysosome (Figure 5E and F). These results confirm that the INR@FRT has a high cell uptake ratio and good mitochondrial targeting. Most importantly, it demonstrated that after entering cells, INR@FRT as a DDDS could first locate at the lysosomes; under acidic conditions, INR was released to the cytoplasm and then targeted the mitochondrion. The DDDS is more efficient for drug precise delivery. This specific mechanism can be presumed to be mediated by active transport and lipophilic cations mediated by organic-anion

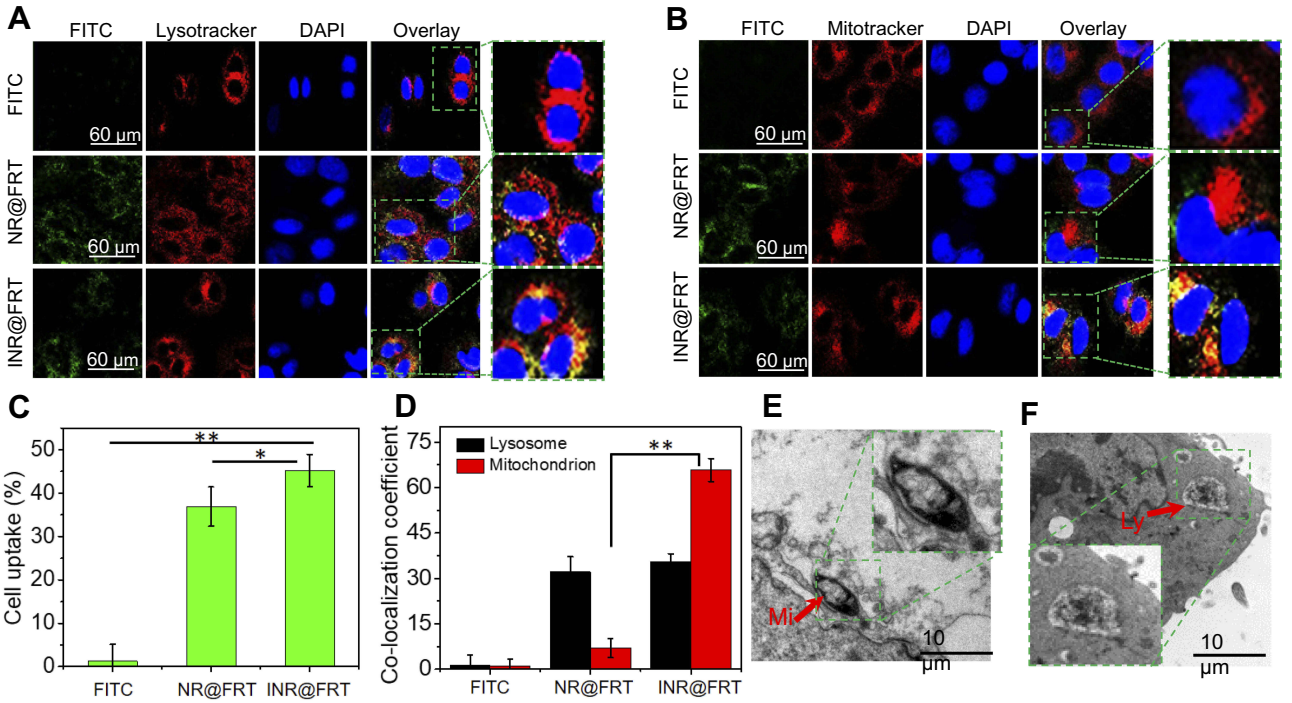

Figure 5 (**A** and **B**) The fluorescence images of SKOV-3 cells incubated with FITC-labeled NR@FRT and INR@FRT for 4 hrs. Scale bar=60 μm. (**C**) Flow cytometry measurement of cellular FITC fluorescence intensities in SKOV-3 cells after incubation with free FITC and FITC-labeled NR@FRT and INR@FRT. *P<0.05, **P<0.01. (**D**) The corresponding co-localization coefficient of FITC-labeled FITC-labeled NR@FRT and INR@FRT with lysosome and mitochondria in cells in A and B. **P<0.01. (**E** and **F**) The bio-TEM image of INR@FRT treated cells.

Abbreviations: NGO, nanosized graphene oxide; FRT, ferritin; IR780, IR-780 iodide; RSV, resveratrol; FITC, fluorescein isothiocyanate; DAPI, 4′,6-diamidino-2-phenylindole; MI, mitochondria; Ly, lysosome.

transport polypeptides, which in turn promotes targeting of nanoparticles to the mitochondria.[40–42]

In vitro Synergistic Cancer Photothermal-Chemotherapy

Figure 6A and B show the temperature of adherent SKOV-3 cells incubated with PBS, NR@FRT, and INR@FRT under an 808 nm irradiation (0.3 W cm^{-2}) for 3 min. The results showed that the cells treated with INR@FRT had the highest temperature increase (ΔT = 30°C) compared to that treated with PBS and NR@FRT-treated cells. For the biocompatibility of the DDDS, IN@FRT with a high concentration up to 0.5 mg/mL showed no significant cell viability at 24 h and 48 h (Figure 6C). The viabilities of the cells treated with various concentrations of RSV, NR@FRT, and INR@FRT for 24 h and 48 h with or without NIR irradiation were concentration-dependent and the viability decreased with increasing concentration. The highest cell viability decrease was observed in INR@FRT + NIR and 48 h-treated cells, which was about 97.2 ± 2.1% (Figure 6D–F). The results demonstrated that the combination of INR@FRT and NIR had an excellent anti-cancer effect. The mechanism of the tumor therapy can be concluded with two steps: 1) INR@FRT entered the cells, located in the lysosomes, and triggered the release of INR by the acidic environment of the lysosomes; 2) INR targeted the mitochondrion and was triggered to release RSV by NIR-induced heat; 3) The released RSV and hyperthermia synergistically killed the cancer cells.

Cell Apoptosis and MMP Detection

As shown in Figure 7A, the control and IN@FRT-treated cells displayed green fluorescence, suggesting no cytotoxic properties. In the INR@FRT and IN@FRTS-treated groups, most of the dead cells showed red fluorescence, likely due to the chemotherapy and photothermal therapy. However, INR@FRT combined with NIR irradiation killed almost the all cells, showing an excellent synergistic cancer photothermal-chemotherapy.

An annexin V-FITC/PI double staining kit was utilized to detect the type of cell death induced by INR@FRT. As shown in Figure 7B and C, the cells treated with control and IN@FRT showed hardly any dead cells. In the INR@FRT, IN@FRTS + NIR, and INR@FRT + NIR-treated groups, the apoptosis rate was 61.3 ± 2.6%, 72.7 ± 3.1% and 96.8 ± 3.3%, respectively (Figure 7C). These findings suggest that the INR@FRT + NIR killed cancer

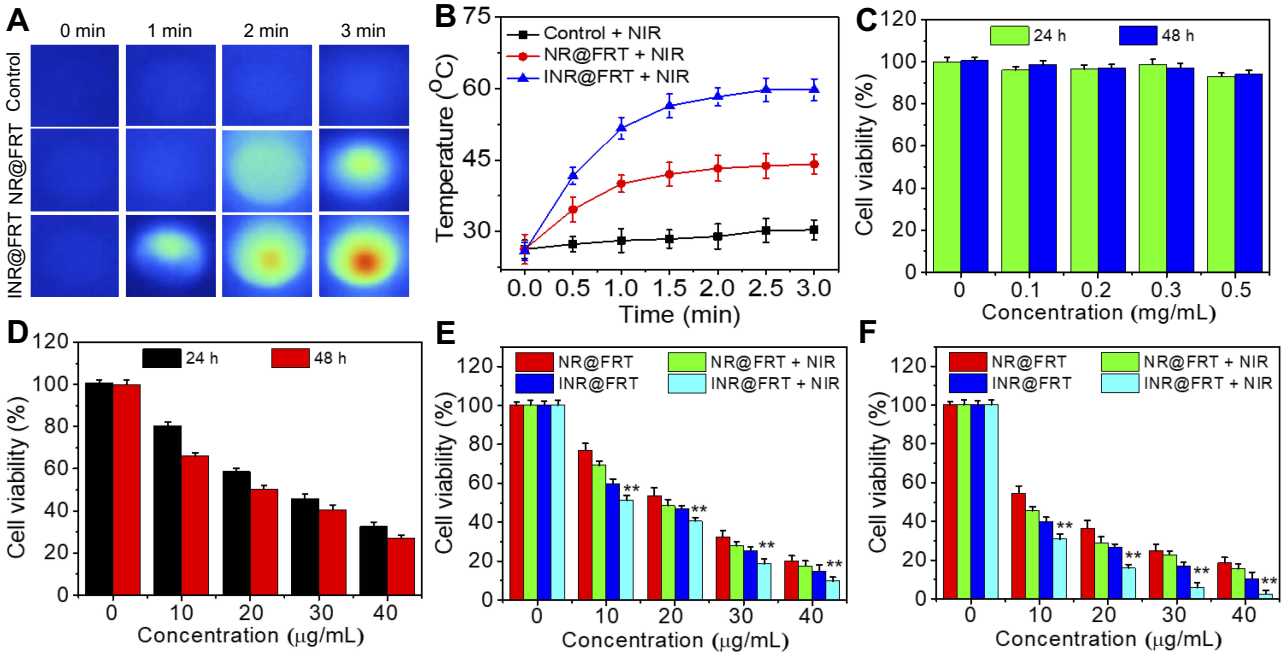

Figure 6 (**A**) Thermal images of PBS, NR@FRT, and INR@FRT treated cells after 3 min NIR irradiation, and (**B**) the corresponding temperature change curves. (**C**) In vitro cytotoxicity against SKOV-3 cells treated with different concentrations of INR@FRT for 24 h and 48 h. (**D**) In vitro cytotoxicity against SKOV-3 cells treated with different concentrations of RSV for 24 h and 48 h. In vitro cytotoxicity against SKOV-3 cells treated with different concentrations of NR@FRT and INR@FRT with or without NIR irradiation for (**E**) 24 h and (**F**) 48 h. $^{**}P<0.01$, vs the other groups at the same concentration.

Abbreviations: NGO, nanosized graphene oxide; FRT, ferritin; IR780, IR-780 iodide; RSV, resveratrol; NIR, near-infrared.

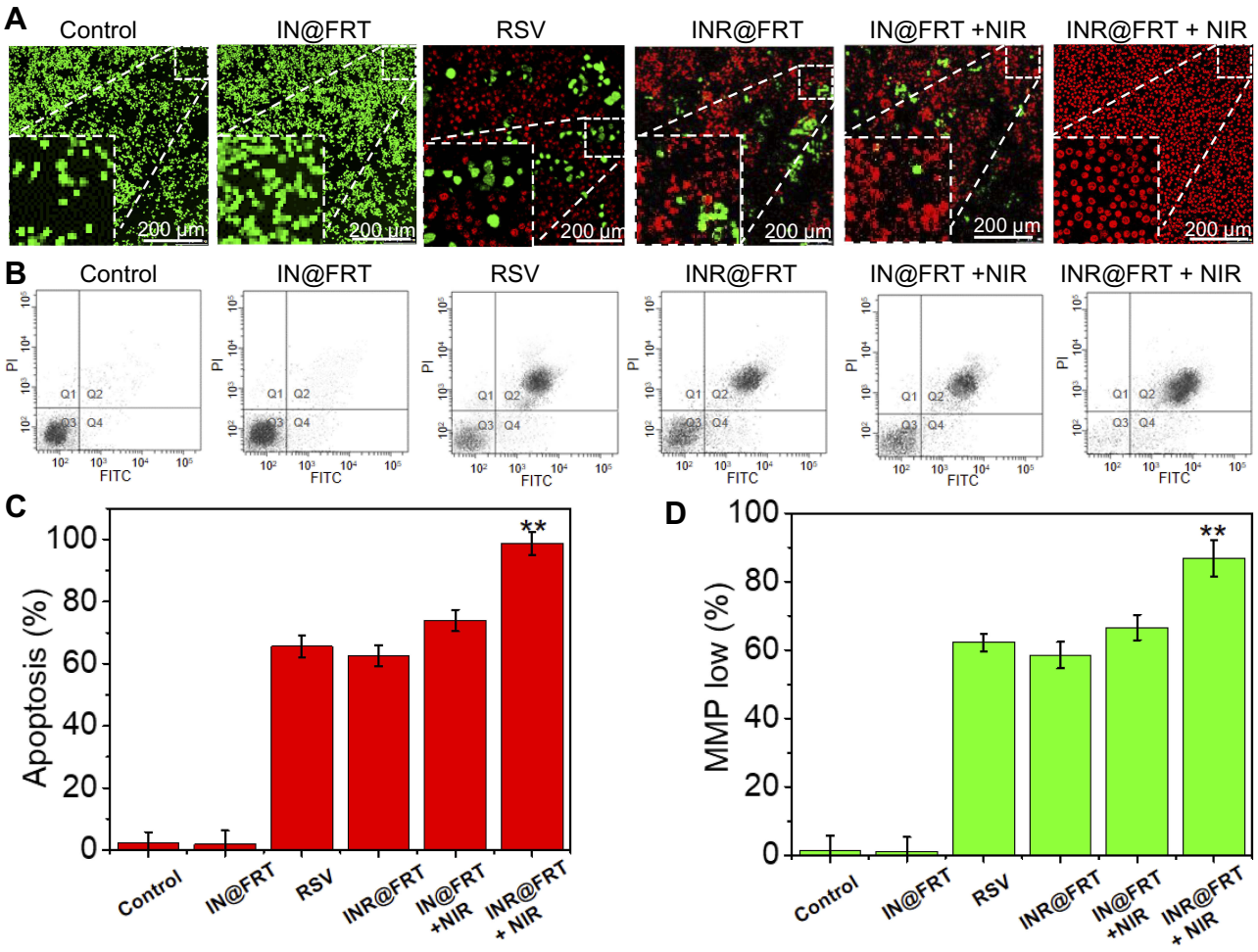

Figure 7 (**A**) The calcium AM/PI dual-staining images of cells after treatment by control (PBS), free RSV, IN@FRT, INR@FRT, NR@FRT + NIR, and INR@FRT + NIR (with the same RSV concentration 40 μg/mL) for 48 h, respectively. (**B**) Cell apoptosis and (**C**) corresponding apoptosis rate of cells treated with PBS (control), free RSV, IN@FRT, INR@FRT, NR@FRT + NIR, and INR@FRT + NIR (with the same RSV concentration 40 μg/mL) for 48 h by flow cytometry, respectively. $^{**}P<0.01$, vs the other groups. (**D**) The change of MMP of SKOV-3 cells treated with PBS (control), free RSV, IN@FRT, INR@FRT, NR@FRT + NIR, and INR@FRT + NIR (with the same RSV concentration 40 μg/mL) for 48 h by flow cytometry, respectively. The NIR irradiation uses 808 nm laser at 0.3 W/cm^2 for 3 min. $^{**}P<0.01$, vs the other groups.

Abbreviations: NGO, nanosized graphene oxide; FRT, ferritin; IR780, IR-780 iodide; RSV, resveratrol; NIR, near infrared; MMP, mitochondrial membrane potential.

cells mediated by apoptosis, likely because of the released RSV in the cytoplasm.[43–45]

Mitochondrion play an important role in cell apoptosis. The decrease of MMP has been reported as the key event in the mitochondrial (intrinsic) apoptotic pathway. As shown in Figure 7D, in the INR@FRT, IN@FRTS + NIR, and INR@FRT + NIR-treated groups, the MMP showed a 59.4 ± 3.5%, 68.3 ± 3.2% and 89.8 ± 4.1% decrease, respectively. From these results, it can be concluded that the INR@FRT + NIR induced cell death that was mediated via the mitochondrial (intrinsic) apoptotic pathway.[46–49]

In vivo Blood Circulation and Biodistribution

Figure 8A shows the blood circulation time of free RSV and INR@FRT after intravenous injecting into mice. INR@FRT displayed the half-life time of 7.13 ±0.3 h. While free RSV was quickly removed from the blood-circulating system ($t_{1/2}$=1.36 ±0.65 h). The blood circulation time of free RSV was highly prolonged, mainly due to the PEG and FRT encapsulation. Furthermore, 24 h post-injection with the nanoparticles, the content of RSV in the tumor and major organs tissue was investigated. As shown in Figure 8B, in the major organs, the nanoparticles mainly accumulated in liver, indicating that these nanoparticles were mainly metabolized through a hepatic pathway. In addition, higher content of INR@FRT was detected in the tumor tissue compared with that of NR@FRT, because of the enhanced permeability and retention (EPR) and the IR780 targeting effect to mitochondrion.

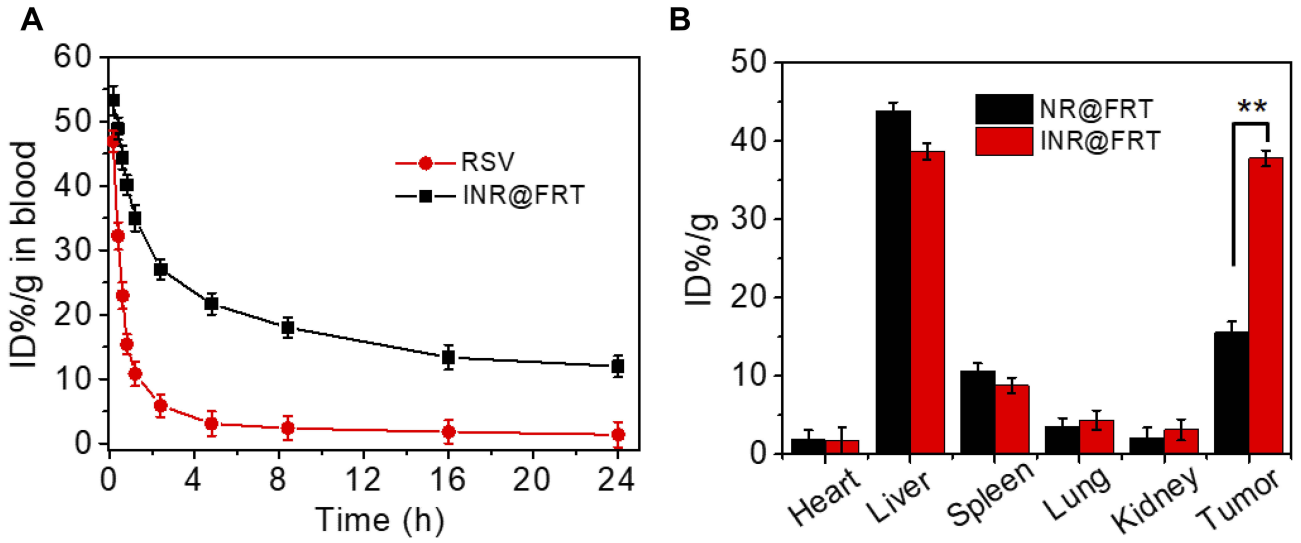

Figure 8 (**A**) Blood circulation curves of free RSV and INR@FRT in mice after intravenous injection determined by the RSV absorbance from diluted tissue lysate (The accumulation of RSV was calculated to be ID% per gram (the percentage of the injected dose per gram of tissue). (**B**) Content of NR@FRT and INR@FRT in major organs and tumor at 24 h post-treatment with nanoparticles determined by the RSV absorbance from diluted tissue lysate. $^{**}P<0.01$.

In vivo Synergistic Cancer Photothermal-Chemotherapy

Encouraged by the excellent in-vitro synergistic cancer therapy, an in-vivo tumor therapy was investigated in an animal model. SKOV-3 xenografted tumors were generated in nude mice and divided into 7 random groups which were treated with PBS, RSV, IN@FRT, NR@FRT, INR@FRT, NR@FRT +NIR, and INR@FRT + NIR, respectively. The NIR irradiation was conducted at 12 h and 24 h post-injection. During the 3 mins of NIR irradiation, the highest temperature increase of 25°C was observed in the INR@FRT - treated tumor, which was higher than that of the PBS (control) and the NR@FRT treated tumors (Figure 9A and B). After treatment for 1 month, the body weight of all the groups showed no significant decrease (Figure 9C). For their relative tumor volume, compared to other groups including PBS, RSV, IN@FRT, NR@FRT, INR@FRT, NR@FRT +NIR, INR@FRT +NIR exhibited excellent tumor suppression without relapse (Figure 9D). Furthermore, after 2 months of initial treatment, the survival rate of mice in the INR@FRT +NIR-treated group had a 100% survival rate, which was higher than that of the other groups (Figure 9E). Figure 9F shows the HE staining images of tumor tissue. A large area of apoptosis was observed in tumors treated with INR@FRT + NIR compared to other groups. Moreover, major organs, including the lung, heart, liver, spleen, and kidney in these treated groups, were harvested for histological analysis. As shown in Figure 9G, the H&E stained sections of INR@FRT +NIR showed no noticeable organ damage when compared with those of the control group. These results indicated that INR@FRT combined with NIR irradiation had splendid biocompatibility features and excellent in-vivo anticancer efficacy mostly due to the precise targeting of organelles and high-efficient pH/heat triggered drug release.[50–55] The results demonstrated that the INR@FRT has no significant cytotoxicity in vivo, which indicates its excellent biocompatibility.

Conclusion

In summary, we have designed and prepared a multifunctional INR@FRT DDDS based on the FRT protein and the NGO. In this system, the NGO sheets, as the first drug carrier, highly loaded RSV and conjugated mitochondrion IR780 to form INR. FRT, as the second carrier, capsulated the INR via the disassembly of FRT under acidic conditions. The resulted INR@FRT showed excellent physiological stability and biocompatibility. Due to the contribution of IR780 and NGO to NIR absorbance, INR@FRT was confirmed to be a splendid photothermal agent. Under the acidic conditions, FRT disassembled to release the INR. NIR irradiation triggers RSV release from NGO; and after entering cells, INR@FRT enters the lysosomes, providing an acidic environment to trigger FRT release of

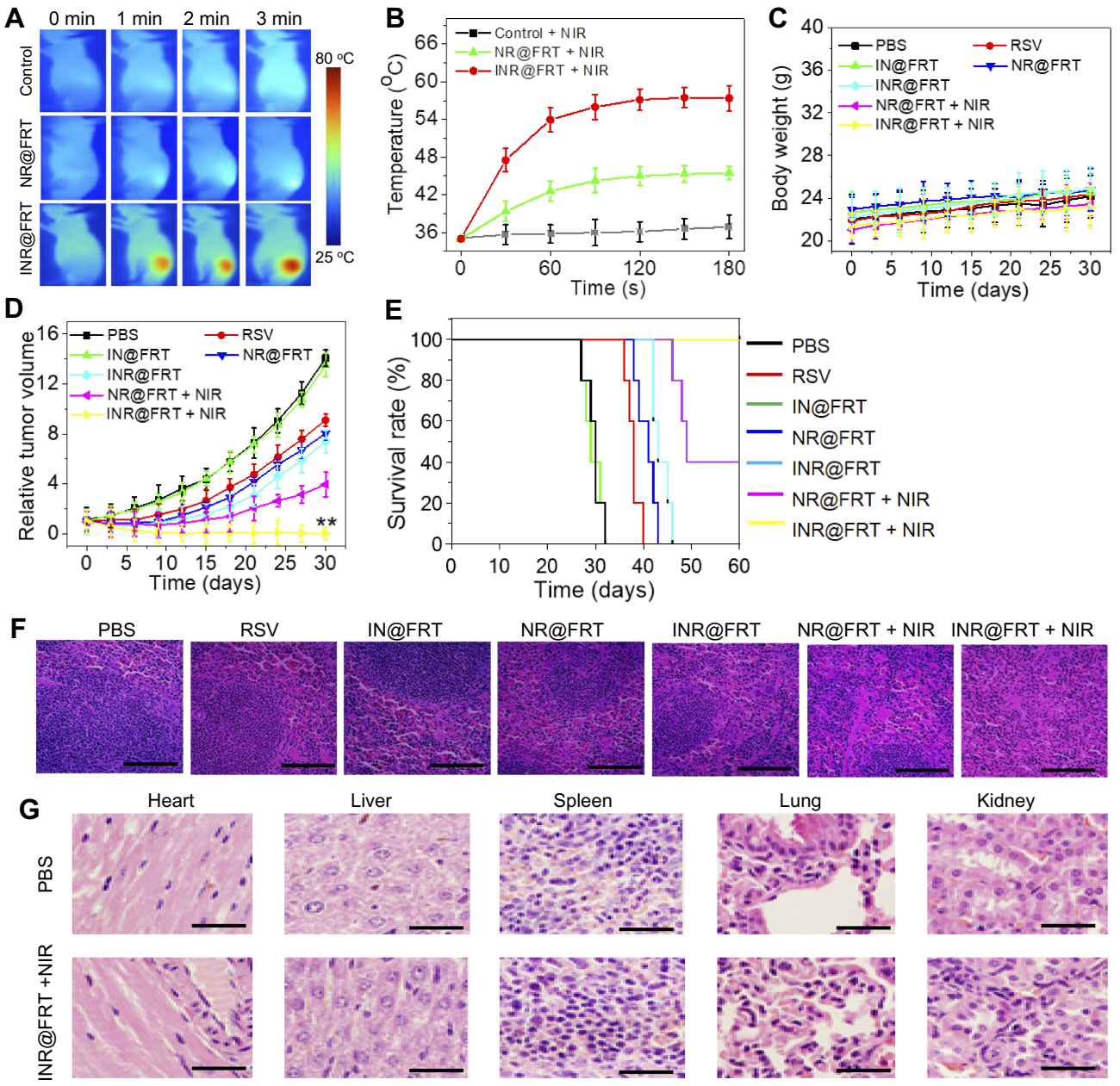

Figure 9 (**A**) The thermal images and (**B**) corresponding temperature statistical results of tumor-bearing mice post-tail vein injection of control PBS, NR@FRT and INR@FRT at 24 h under 3 min NIR irradiation (808 nm, 0.3 W/cm^2), respectively. (**C**) Body weight of tumor-bearing mice after various treatments. (**D**) The growth profile of SKOV-3 xenografted tumors after intravenous injection of PBS, RSV, IN@FRT, NR@FRT, INR@FRT, NR@FRT + NIR and INR@FRT + NIR (808 nm, 0.3 W/cm^2). **P<0.01, vs the other groups. (**E**) The survival rate of tumor-bearing mice after various treatments for 60 days. (**F**) Micrographs of H&E-stained tumor slices collected from PBS-, RSV-, IN@FRT-, NR@FRT-, INR@FRT-, NR@FRT + NIR- and INR@FRT + NIR- (808 nm, 0.3 W/cm^2) treated groups at the end of the treatment. Scale bar = 50 μm. (**G**) H&E-stained tissue sections of major organs, including the heart, liver, spleen, lung, and kidney from tumor-bearing mice in saline (control) and INR@FRT + NIR groups after the treatment. Scale bar = 100 μm.

Abbreviations: NGO, nanosized graphene oxide; FRT, ferritin; IR780, IR-780 iodide; RSV, resveratrol; NIR, near-infrared.

INR. With the guidance of IR780, INR targeted the mitochondrion and released RSV under the NIR irradiation. The multifunctional INR@FRT accompanied with pH/heat-triggered RSV release showed a great synergistic suppression of tumor growth both in-vitro and in-vivo without systemic toxicity. These results demonstrate that the INR@FRT can be a potential and high-efficiency DDDS for cancer therapy.

Disclosure

The authors report no conflicts of interest in this work.

References

1. Miller KD, Siegel RL, Lin CC, et al. Cancer treatment and survivorship statistics, 2016. *CA Cancer J Clin*. 2016;66(4):271–289. doi:10.3322/caac.21349
2. Matulonis UA, Sood AK, Fallowfield L, Howitt BE, Sehouli J, Karlan BY. Ovarian cancer. *Nat Rev Dis Primers*. 2016;2:16061. doi:10.1038/nrdp.2016.61
3. Korach J, Colombo N, Mendiola C, et al. Outcome according to residual disease (surgeon's report vs pre-chemotherapy imaging) in patients with bevacizumab-treated ovarian cancer: analysis of the ROSiA study. *J Surg Oncol*. 2019. doi:10.1002/jso.25647
4. Kumari P, Ghosh B, Biswas S. Nanocarriers for cancer-targeted drug delivery. *J Drug Target*. 2016;24(3):179–191. doi:10.3109/1061186X.2015.1051049
5. Zhang W, Wang G, Falconer JR, et al. Strategies to maximize liposomal drug loading for a poorly water-soluble anticancer drug. *Pharm Res*. 2015;32(4):1451–1461. doi:10.1007/s11095-014-1551-8
6. Kim DS, Cho JH, Park JH, et al. Self-microemulsifying drug delivery system (SMEDDS) for improved oral delivery and photostability of methotrexate. *Int J Nanomedicine*. 2019;14:4949. doi:10.2147/IJN.S211014
7. Wang CF, Sarparanta MP, Mäkilä EM, et al. Multifunctional porous silicon nanoparticles for cancer theranostics. *Biomaterials*. 2015;48:108–118. doi:10.1016/j.biomaterials.2015.01.008
8. Yang J, Teng Y, Fu Y, Zhang C. Chlorins e6 loaded silica nanoparticles coated with gastric cancer cell membrane for tumor specific photodynamic therapy of gastric cancer. *Int J Nanomedicine*. 2019;14:5061. doi:10.2147/IJN.S202910
9. Tahir N, Madni A, Correia A, et al. Lipid-polymer hybrid nanoparticles for controlled delivery of hydrophilic and lipophilic doxorubicin for breast cancer therapy. *Int J Nanomedicine*. 2019;14:4961. doi:10.2147/IJN.S209325
10. Kanamala M, Wilson WR, Yang M, Palmer BD, Wu Z. Mechanisms and biomaterials in pH-responsive tumour targeted drug delivery: a review. *Biomaterials*. 2016;85:152–167. doi:10.1016/j.biomaterials.2016.01.061
11. Zheng Y, You X, Guan S, et al. Poly (Ferulic Acid) with an anticancer effect as a drug nanocarrier for enhanced colon cancer therapy. *Adv Funct Mater*. 2019;29(15):1808646. doi:10.1002/adfm.201808646
12. Zheng Y, You X, Chen L, et al. Biotherapeutic nanoparticles of poly (Ferulic Acid) delivering doxorubicin for cancer therapy. *J Biomed Nanotechnol*. 2019;15(8):1734–1743. doi:10.1166/jbn.2019.2798
13. Zhang X, Zhang R, Huang J, et al. Albumin enhances PTX delivery ability of dextran NPs and therapeutic efficacy of PTX for colorectal cancer. *J Mater Chem B*. 2019;7:3537–3545. doi:10.1039/C9TB00181F
14. Zhang X, Kang Y, Liu G, et al. Poly (cystine–PCL) based pH/redox dual-responsive nanocarriers for enhanced tumor therapy. *Biomater Sci*. 2019;7(5):1962–1972. doi:10.1039/C9BM00009G
15. Wen J, Yang K, Liu F, Li H, Xu Y, Sun S. Diverse gatekeepers for mesoporous silica nanoparticle based drug delivery systems. *Chem Soc Rev*. 2017;46(19):6024–6045. doi:10.1039/c7cs00219j
16. Hughes GA. Nanostructure-mediated drug delivery. *Nanomedicine*. 2005;1(1):22–30. doi:10.1016/j.nano.2004.11.009
17. Chen T, Wu W, Xiao H, Chen Y, Chen M, Li J. Intelligent drug delivery system based on mesoporous silica nanoparticles coated with an ultra-pH-sensitive gatekeeper and poly (ethylene glycol). *ACS Macro Lett*. 2015;5(1):55–58. doi:10.1021/acsmacrolett.5b00765
18. Cheng YJ, Luo GF, Zhu JY, et al. Enzyme-induced and tumor-targeted drug delivery system based on multifunctional mesoporous silica nanoparticles. *ACS Appl Mater Interfaces*. 2015;7(17):9078–9087. doi:10.1021/acsami.5b00752
19. Lim DJ, Sim M, Oh L, Lim K, Park H. Carbon-based drug delivery carriers for cancer therapy. *Arch Pharm Res*. 2014;37(1):43–52. doi:10.1007/s12272-013-0277-1
20. Chen J, Liu H, Zhao C, et al. One-step reduction and PEGylation of graphene oxide for photothermally controlled drug delivery. *Biomaterials*. 2014;35(18):4986–4995. doi:10.1016/j.biomaterials.2014.02.032
21. Pattni BS, Chupin VV, Torchilin VP. New developments in liposomal drug delivery. *Chem Rev*. 2015;115(19):10938–10966. doi:10.1021/acs.chemrev.5b00046
22. Pardridge WM. Blood–brain barrier drug delivery of IgG fusion proteins with a transferrin receptor monoclonal antibody. *Expert Opin Drug Deliv*. 2015;12(2):207–222. doi:10.1517/17425247.2014.952627
23. Wu W, Yao W, Wang X, Xie C, Zhang J, Jiang X. Bioreducible heparin-based nanogel drug delivery system. *Biomaterials*. 2015;39:260–268. doi:10.1016/j.biomaterials.2014.11.005
24. Xiao W, Zeng X, Lin H, Han K, Jia HZ, Zhang XZ. Dual stimuli-responsive multi-drug delivery system for the individually controlled release of anti-cancer drugs. *Chem Commun*. 2015;51(8):1475–1478. doi:10.1039/c4cc08831j
25. Karimi M, Ghasemi A, Zangabad PS, et al. Smart micro/nanoparticles in stimulus-responsive drug/gene delivery systems. *Chem Soc Rev*. 2016;45(5):1457–1501. doi:10.1039/c5cs00798d
26. Loira-Pastoriza C, Todoroff J, Vanbever R. Delivery strategies for sustained drug release in the lungs. *Adv Drug Deliv Rev*. 2014;75:81–91. doi:10.1016/j.addr.2014.05.017
27. Jutz G, van Rijn P, Santos Miranda B, Böker A. Ferritin: a versatile building block for bionanotechnology. *Chem Rev*. 2015;115(4):1653–1701. doi:10.1021/cr400011b
28. Huang P, Rong P, Jin A, et al. Dye-loaded ferritin nanocages for multimodal imaging and photothermal therapy. *Adv Mater*. 2014;26(37):6401–6408. doi:10.1002/adma.201400914
29. Liang M, Fan K, Zhou M, et al. H-ferritin–nanocaged doxorubicin nanoparticles specifically target and kill tumors with a single-dose injection. *Proc Natl Acad Sci U S A*. 2014;111(41):14900–14905. doi:10.1073/pnas.1407808111
30. Truffi M, Fiandra L, Sorrentino L, Monieri M, Corsi F, Mazzucchelli S. Ferritin nanocages: a biological platform for drug delivery, imaging and theranostics in cancer. *Pharmacol Res*. 2016;107:57–65. doi:10.1016/j.phrs.2016.03.002
31. Yang K, Feng L, Liu Z. The advancing uses of nano-graphene in drug delivery. *Expert Opin Drug Deliv*. 2015;12(4):601–612. doi:10.1517/17425247.2015.978760
32. Goenka S, Sant V, Sant S. Graphene-based nanomaterials for drug delivery and tissue engineering. *J Control Release*. 2014;173:75–88. doi:10.1016/j.jconrel.2013.10.017
33. Li J, Lyv Z, Li Y, et al. A theranostic prodrug delivery system based on Pt (IV) conjugated nano-graphene oxide with synergistic effect to enhance the therapeutic efficacy of Pt drug. *Biomaterials*. 2015;51:12–21. doi:10.1016/j.biomaterials.2015.01.074
34. Beik J, Abed Z, Shakeri-Zadeh A, Nourbakhsh M, Shiran MB. Evaluation of the sonosensitizing properties of nano-graphene oxide in comparison with iron oxide and gold nanoparticles. *Physica E*. 2016;81:308–314. doi:10.1016/j.physe.2016.03.023
35. Beik J, Abed Z, Ghadimi-Daresajini A, et al. Measurements of nanoparticle-enhanced heating from 1 MHz ultrasound in solution and in mice bearing CT26 colon tumors. *J Therm Biol*. 2016;62:84–89. doi:10.1016/j.jtherbio.2016.10.007
36. Beik J, M B S, Abed Z, et al. Gold nanoparticle-induced sonosensitization enhances the antitumor activity of ultrasound in colon tumor-bearing mice. *Med Phys*. 2018;45(9):4306–4314. doi:10.1002/mp.13100
37. Beik J, Khademi S, Attaran N, et al. A nanotechnology-based strategy to increase the efficiency of cancer diagnosis and therapy: folate-conjugated gold nanoparticles. *Curr Med Chem*. 2017;24(39):4399–4416. doi:10.2174/0929867324666170810154917
38. Niu X, Gao Z, Qi S, et al. Macropinocytosis activated by oncogenic Dbl enables specific targeted delivery of Tat/pDNA nano-complexes into ovarian cancer cells. *Int J Nanomedicine*. 2018;13:4895–4911. doi:10.2147/IJN.S171361

39. Arosio P, Ingrassia R, Cavadini P. Ferritins: a family of molecules for iron storage, antioxidation and more. *Biochim Biophys Acta Gen Subj*. 2009;1790(7):589–599. doi:10.1016/j.bbagen.2008.09.004
40. Xiang S, Zhang K, Yang G, Gao D, Zeng C, Mitochondria-Targeted HM. Resveratrol-loaded dual-function titanium disulfide nanosheets for photothermal-triggered tumor chemotherapy. *Nanoscale Res Lett*. 2019;14(1):211. doi:10.1186/s11671-019-3044-5
41. Guo F, Yu M, Wang J, Tan F, Li N. The mitochondria-targeted and IR780-regulated theranosomes for imaging and enhanced photodynamic/photothermal therapy. *RSC Adv*. 2016;6(14):11070–11076. doi:10.1039/C5RA19521G
42. Zhang E, Luo S, Tan X, Shi C. Mechanistic study of IR-780 dye as a potential tumor targeting and drug delivery agent. *Biomaterials*. 2014;35(2):771–778. doi:10.1016/j.biomaterials.2013.10.033
43. Zhou JH, Cheng HY, Yu ZQ, He DW, Zheng PA, Yang DT. Resveratrol induces apoptosis in pancreatic cancer cells. *Chinese Med J*. 2011;124(11):1695.
44. Surh YJ, Hurh YJ, Kang JY, Lee E, Kong G, Lee SJ. Resveratrol, an antioxidant present in red wine, induces apoptosis in human promyelocytic leukemia (HL-60) cells. *Cancer Lett*. 1999;140(1–2):1–10. doi:10.1016/s0304-3835(99)00039-7
45. Li Q, Yue Y, Chen L, et al. Resveratrol sensitizes carfilzomib-induced apoptosis via promoting oxidative stress in multiple myeloma cells. *Front Pharmacol*. 2018;9:334. doi:10.3389/fphar.2018.00334
46. Hao Q, Xiao X, Zhen J, et al. Resveratrol attenuates acute kidney injury by inhibiting death receptor-mediated apoptotic pathways in a cisplatin-induced rat model. *Mol Med Rep*. 2016;14(4):3683–3689. doi:10.3892/mmr.2016.5714
47. Zhao H, Han L, Jian Y, et al. Resveratrol induces apoptosis in human melanoma cell through negatively regulating Erk/PKM2/Bcl-2 axis. *Onco Targets Ther*. 2018;11:8995. doi:10.2147/OTT.S186247
48. Arif W, Xu S, Isailovic D, et al. Complexes of the outer mitochondrial membrane protein mitoNEET with resveratrol-3-sulfate. *Biochemistry*. 2011;50(25):5806–5811. doi:10.1021/bi200546s
49. Kalra N, Roy P, Prasad S, Shukla Y. Resveratrol induces apoptosis involving mitochondrial pathways in mouse skin tumorigenesis. *Life Sci*. 2008;82(7–8):348–358. doi:10.1016/j.lfs.2007.11.006
50. Alamzadeh Z, Beik J, V P M, et al. Ultrastructural and optical characteristics of cancer cells treated by a nanotechnology based chemo-photothermal therapy method. *J Photochem Photobiol B*. 2019;192:19–25. doi:10.1016/j.jphotobiol.2019.01.005
51. Mirrahimi M, Abed Z, Beik J, et al. A thermo-responsive alginate nanogel platform co-loaded with gold nanoparticles and cisplatin for combined cancer chemo-photothermal therapy. *Pharmacol Res*. 2019;143:178–185. doi:10.1016/j.phrs.2019.01.005
52. Beik J, Khateri M, Khosravi Z, et al. Gold nanoparticles in combinatorial cancer therapy strategies. *Coord Chem Rev*. 2019;387:299–324. doi:10.1016/j.ccr.2019.02.025
53. Neshastehriz A, Tabei M, Maleki S, Eynali S, Shakeri-Zadeh A. Photothermal therapy using folate conjugated gold nanoparticles enhances the effects of 6 MV X-ray on mouth epidermal carcinoma cells. *J Photochem Photobiol B*. 2017;172:52–60. doi:10.1016/j.jphotobiol.2017.05.012
54. Ghaznavi H, Hosseini-Nami S, S K K, et al. Folic acid conjugated PEG coated gold–iron oxide core–shell nanocomplex as a potential agent for targeted photothermal therapy of cancer. *Artif Cells Nanomed Biotechnol*. 2018;46(8):1594–1604. doi:10.1080/21691401.2017.1384384
55. Mirrahimi M, Hosseini V, S K K, et al. Selective heat generation in cancer cells using a combination of 808 nm laser irradiation and the folate-conjugated Fe2O3@ Au nanocomplex. *Artif Cells Nanomed Biotechnol*. 2018;46(sup1):241–253. doi:10.1080/21691401.2017.1420072